Modularized Electrosurgical System With a Hybrid CPU-FPGA Chip for Real-Time Thermal Lesion Approximation

Jinhwan Baik, Sangyong Lee, Sunchoel Yang, and Sung-Min Park, *Senior Member, IEEE*

***Abstract*— Electrosurgery that ablates the target tissues such as tumor and nerve cells using radio-frequency (RF) heating has been widely employed in the medical industry. Although the thermal lesion plays a key role in the efficacy and safety for this method, it is still difficult to identify the depth and size of the lesion during the treatment using recent electrosurgical systems. Herein, we propose a novel electrosurgical instrument for real-time approximation of thermal lesions during RF ablation (RFA). Thermal lesions were numerically calculated based on theoretical thermal models using a hybrid central processing unit (CPU)-field-programmable gate array (FPGA) chip. Other functions such as RF control, voltage, and temperature measurements were implemented using RF components in a modular manner. It can solve voltage distribution in 6 ms by repeating the calculation 5000 times and can anticipate the thermal lesion in 15.6 ms within a time step in real-time simulations. As a real-world validation, the feasibility of the system was demonstrated through an animal study using a swine model. The system is modularly designed using off-the-shelf chips and RF components to improve flexibility and scalability. It can be easily compatible with existing RF surgical applications and medical imaging devices and can improve the efficacy of RFA therapy.**

***Index Terms*— Field-programmable gate array (FPGA), finite-difference time domain (FDTD), real-time numerical simulation, radio-frequency ablation (RFA), renal denervation.**

Manuscript received November 15, 2021; revised January 23, 2022; accepted February 14, 2022. Date of publication February 25, 2022; date of current version March 16, 2022. This work was supported in part by the Basic Science Research Program through the National Research Foundation of Korea (NRF) funded by the Ministry of Education under Grant 2020R1A6A3A13066375 and Grant 2020R1A6A1A03047902; in part by the National Research Foundation of Korea (NRF) funded by the Ministry of Science and ICT (MSIT), Korea Government, under Grant NRF-2017R1A5A1015596; and in part by the National Research and Development Program through the National Research Foundation of Korea (NRF) funded by the Ministry of Science and ICT under Grant 2021M3H4A1A03049084. The Associate Editor coordinating the review process was Dr. Tarikul Islam. *(Corresponding author: Sung-Min Park.)*

This work involved human subjects or animals in its research. Approval of all ethical and experimental procedures and protocols was granted by Institutional Animal Care and Use Committee in the Osong Medical Innovation Foundation under Approval No. KBIO-IACUC-2021-221.

Jinhwan Baik is with the Department of Convergence IT Engineering and the Medical Device Innovation Center, Pohang University of Science and Technology (POSTECH), Pohang 37673, Republic of Korea (e-mail: jinhwan52@postech.ac.kr).

Sangyong Lee and Sunchoel Yang are with the Department of Prototype Production, Osong Medical Innovation Foundation, Cheongju-si, Chungbuk 28160, Republic of Korea (e-mail: lsy@kbiohealth.kr; ysc@kbiohealth.kr).

Sung-Min Park is with the Department of Convergence IT Engineering, the Department of Electrical Engineering, the Department of Mechanical Engineering, and the Medical Device Innovation Center, Pohang University of Science and Technology (POSTECH), Pohang 37673, Republic of Korea (e-mail: sungminpark@postech.ac.kr).

Digital Object Identifier 10.1109/TIM.2022.3154817

I. Introduction

In the medical industry, electrosurgery, which generates heat from tissue using radio-frequency (RF) energy, called RF ablation (RFA) surgery, has considerably improved the operational efficiency and postoperative recovery [1]. RFA has been widely employed in minimally invasive surgery using robotic, laparoscopic, and endoscopic system [2], [3]. It can effectively ablate the target tumor or nerve cells in the brain [4], liver [5], spinal cord [6], and vascular tissues [7]. An important requirement for effective RFA procedures is the capability of localizing heat on the target tissues to minimize irreversible damage to adjacent normal tissues, which is a critical side effect of any thermal treatment. Therefore, surgeons should pre-plan the details of RFA applications to avoid thermal injury and to improve the effectiveness of treatment.

Using theoretical models about RFA [8], offline simulation tools (e.g., ANSYS, COMSOL, and Sim4life) can analyze the electrical and thermal effects of RFA applications using CT or MRI results of patients [9], [10]. Such tools, which perform predictive analysis of RFA results under various surgical environments considering the structure of a patient's organs, tissue conditions, blood flow, or perfusions, have proved to be useful for improving the clinical outcomes of the procedure. However, during surgery, anatomical variations that could not be identified with conventional imaging devices and unexpected physiological variations such as blood flow and conductivity make the accurate prediction of the thermal damage caused by the electrosurgical system difficult before the treatment. Therefore, the thermal lesion during RFA must be approximated while considering the various surgical environments more realistically.

Recent electrosurgical instrument controlled by a microcontroller unit (MCU) can monitor the electrode temperature and transmitted RF energy during treatment. Some papers have attempted to use bio-impedance spectroscopy to provide information regarding thermal lesions during RFA without imaging devices [11]–[13]. However, this method requires additional RF electrodes and is only applicable to limited organs composed of homogeneous tissue such as the liver. In addition, performing real-time simulations is difficult for MCU-based systems due to their limited processing speed and memory. This feature is possible if the theoretical thermal models are solved numerically within a time step in real-time simulation. Therefore, approximating thermal lesion during

RFA requires in-depth knowledge of the theoretical models of RFA, numerical analysis, high-performance computing, and RF systems. In this context, these technical and clinical unmet needs largely motivated the development of an electrosurgical instrument integrated with real-time approximation of thermal lesions using numerical simulation techniques on a hybrid central processing unit (CPU)-field-programmable gate array (FPGA) chip. FPGA has gained a preferred position in real-time simulation for various industrial applications [14]–[16]. FPGA-based systems can compute complex problems using hardwired computational engines in a parallel manner. In addition, the development of a hybrid CPU-FPGA chip significantly increases the flexibility and lowers development costs. In contrast, by programming the entire system with FPGA, the developer can allocate sequential tasks into the CPU as high-level design and combinational tasks into FPGA as low-level design.

In this study, we developed a novel electrosurgical instrument that can conduct RFA, numerically calculate the voltage distribution during operation, and approximate thermal lesions considering the heat intensity, duration, and tissue type. With these capabilities, the proposed system can adjust the ablation scheme even in real-time, and the effectiveness of the procedure can be optimized further from the preplanning procedure. The main contributions of this study are as follows.

1) We propose a real-time numerical computing procedure on a hybrid CPU-FPGA chip to numerically solve the bio-heat equation by combining the electrical and thermal problem, the results of which are the heat distribution in the tissue. The electrical problem was solved using a dedicated accelerator composed of five-stage pipelined computing units in FPGA. If the electrical and thermal boundary conditions are determined, the heat distribution on a hybrid CPU-FPGA chip can be calculated.
2) The functions of the electrosurgical system such as RF generation, the measurement of electrode temperature and voltage, and the approximation of thermal lesions were modularly implemented using commercially available chips and RF components. The modular design method can improve flexibility and scalability. Each module in the system can be individually compatible with existing electrosurgical systems or medical imaging devices.
3) We developed a novel electrosurgical system consisting of the proposed chip and RF components. The system delivers RF energy to a surgical electrode and monitors the electrical and thermal boundary conditions, such as the electrode temperature, the transmitted RF energy, and the load impedance. Concurrently, the system approximates the thermal lesion considering surgical situations and displays the results on a monitor during surgery. To the best of our knowledge, this is the first study in which an electrosurgical system capable of real-time approximation of thermal lesions on a single chip has been developed.

II. Theoretical Models About RFA

A. Offline Numerical Simulation

To predict the heat distribution during electrosurgery via offline numerical simulation, the first step is to model the physical phenomena in the actual surgical situation. In this step, a simulation domain is defined, and the detailed structure including the electrodes and adjacent tissues is modeled. After designing the models, the mathematical equations governing RFA are arranged. For example, the simulation of RFA consists of two physics (electrical and thermal) fields. The governing equation for computing the electrical field distribution is the Laplace equation which can solve the induced electrical potential (V) distribution

$$\nabla \cdot \sigma \nabla V = 0 \tag{1}$$

where σ is the electrical conductivity

$$Q_J = J \cdot E = \sigma (\nabla V)^2. \tag{2}$$

The electrical potential generates Joule heat (Q_J) in tissue following Ohm's law and is coupled with the thermal field

$$\rho C \frac{\partial T}{\partial t} - \nabla \cdot [k \nabla T] = Q_J - Q_{\text{cooling}}. \tag{3}$$

The governing equation for computing the thermodynamics is the heat conduction in tissue that combines the tissue temperature (T) changes in the time domain (t) with density (ρ) and heat capacity (C), the spatial temperature distribution with tissue thermal conductivity (k), the Joule heat generation term, and the cooling effect term. The cooling effect terms depend on the surgical environment such as air flow, bulky blood flow, or blood perfusion. This multiphysics equation is the so-called bio-heat equation [8], [17]. After setting the electrical and thermal parameters of the designed models, a numerical method such as FDTD can solve the governing equations.

B. Real-Time Thermal Lesion Approximation

To perform online numerical analysis during RFA, a simulation tool should numerically solve the coupled electrical–thermal problems in a few milliseconds before the tissue temperature is changed. As a real-world validation to increase the credibility of this study, we considered our previously developed emerging laparoscopic renal denervation (LRDN) technique, in which a renal artery is wrapped and renal nerves are ablated by generating heat using the RF energy [see Fig. 1(a)] [7]. In LRDN, thermal lesions should be concentrated on the outer arterial wall to damage nerves while protecting the artery from thermal damage. Therefore, monitoring subsurface thermal injury of a renal artery is important for effectiveness and safety of the LRDN. The design methodology of the online simulation applicable to the RF system is divided into five steps.

1) Simplification of the Simulation Model: Reducing computation tasks by simplifying the simulation domain or model should take precedence to solve the numerical problems on a chip that uses limited computational resources. To simplify the model, we analyzed the heat distribution using offline

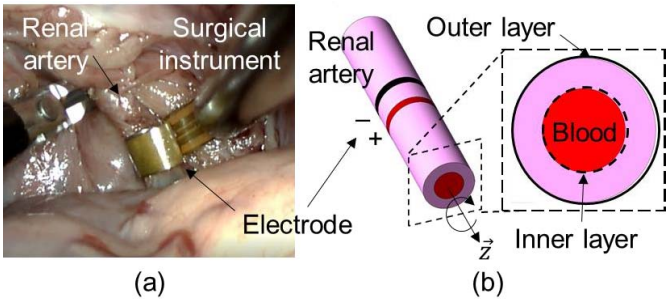

Fig. 1. (a) Actual surgical situation during laparoscopic renal denervation and (b) its simulation model.

numerical simulations and observed the actual surgical situation [7], [9], [18], [19]. In those previous studies, LRDN at the main renal artery without stenosis was analyzed. To simulate the LRDN, the artery was modeled as a cylinder, and the bipolar electrode was modeled as two circular plates (see Fig. 1).

A blood cooling effect occurs on the inner arterial wall; however, the blood perfusion cooling effect is negligible because the renal artery is detached from adjacent fat tissues and capillaries during treatment [20]. Thus, the LRDN model has three unique features: 1) a renal artery (target tissue) and electrodes wrapping the artery can be considered as concentric circles; 2) the simulation model with macro-fragments of the artery and blood is set to be homogeneous; and 3) the surgical electrode is a parallel bipolar electrode which completely wraps a renal artery. From features 1 and 2, the 3-D simulation domain can be simplified into a 2-D cylindrical coordinate system (radial distance r and height z). Feature 3 indicates that the electric field on the outer arterial wall ($\vec{E}_w$) between two parallel electrodes is constant.

We used FDTD to solve the coupled electrical–thermal equation in a 2-D cylindrical coordinate [21]. In this rectangular domain, FDTD has an advantage in terms of mesh generation to solve the linear electrical–thermal equation [22]. Therefore, (1) can be discretized as follows:

$$V_{r,z} = \frac{\Delta r^2 \Delta z^2}{2(\Delta r^2 + \Delta z^2)} \times \left(\frac{1}{r} \frac{V_{r+1,z} - V_{r-1,z}}{2\Delta r} + \frac{V_{r+1,z} + V_{r-1,z}}{\Delta r^2} + \frac{V_{r,z+1} + V_{r,z-1}}{\Delta z^2} \right). \tag{4}$$

In addition, (3) is approximated by employing the second-order central difference scheme for the spatial derivative and the explicit Euler for time advancement

$$T_{r,z}^{f+1} = T_{r,z}^{f} + \frac{k\Delta t}{\rho C} \times \left(\frac{T_{r+1,z}^{f} - T_{r-1,z}^{f}}{2r\Delta r} + \frac{T_{r+1,z}^{f} - 2T_{r,z}^{f} + T_{r-1,z}^{f}}{\Delta r^2} + \frac{T_{r,z+1}^{f} - 2T_{r,z}^{f} + T_{r,z-1}^{f}}{\Delta z^2} \right)$$

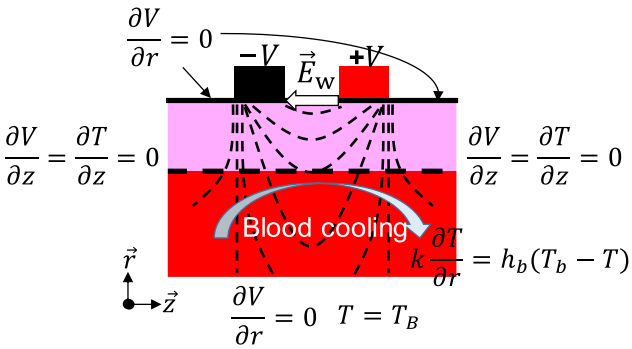

Fig. 2. Cross-sectional view of the modeled bipolar electrosurgery on an artery in a 2-D cylindrical coordinate system (dashed line is an isoline of $|\vec{E}|$).

$$+\frac{k\Delta t}{\rho C} \times \left(\left(\frac{V_{r+1,z} - V_{r-1,z}}{2\Delta r} \right)^2 + \left(\frac{V_{r,z+1} - V_{r,z-1}}{2\Delta z} \right)^2 \right). \tag{5}$$

2) Determination of the Boundary Conditions: Once the simulation model is simplified and the bio-heat equation is discretized, the electrical and thermal boundary conditions must be determined (see Fig. 2). In the electrical field, an electrode–artery interface is set to have a positive or negative electric potential on two parallel electrodes (the Dirichlet boundary condition). Because the electric field between the two electrodes is constant, the potential linearly increases from the cathode to the anode. The other sides of the rectangular domain have a null flux (the Neumann boundary condition). Therefore, to set the electrical boundary condition during RFA, the RF electrosurgical system should measure the voltage on the electrode.

In the thermal field, the blood cooling effect was modeled by a linear cooling law on the artery–blood interface (inner arterial wall) [23]

$$k\frac{\partial T}{\partial r} = h_b(T_b - T), \quad \text{at inner arterial wall} \tag{6}$$

where the temperature of blood (T_b) was 310 K and the convective heat-transfer coefficient of blood (h_b) was 300 W/(m^{2}K). The thermal conductivity of the artery was 0.45 W/(mK) [24]. FDTD solves (4) and (5) numerically in a 2 (r-axis) × 3.85 (z-axis) mm^2 computational domain (Δr = 0.167 mm, Δz = 0.035 mm). In this study, we simulated the cooling effect using a linear cooling law on the artery–blood interface rather than modeling a bulked blood flow. Both of these methods have been used in simulation studies of RFA [8]. We thoroughly examined the effect of these boundary conditions in a previous study [7]. The cooling effect due to the bulked blood flow skewed the heat distribution along the flow direction, whereas the cooling effect due to the linear cooling law did not. However, these two methods identically generated the maximum temperature at the middle of the parallel electrode, which is the main cause of thermal lesion. In addition, in terms of hardware resource on a single chip, such as memory, adaptive logic modules, and DSP, it is better to use the linear cooling law than to use bulky blood

flow when modeling blood cooling effect. The linear cooling law requires only the setting of the boundary condition on the artery–blood interface. However, simulation of the blood cooling effect using blood fluid requires additional calculations and dedicated calculators to solve the conservation of mass and linear momentum. Therefore, the linear cooling law was sufficient to model the clinical effect of LRDN and could reduce the hardware resources used for numerical calculations.

3) Task Allocation to Computational Resources: The bio-heat equation that couples electrical and thermal problems should be solved on a CPU- and FPGA-based chip. Therefore, we decompose the bio-heat equation and solve the electrical problem on FPGA and the thermal problem on the CPU. The electrical problem, which is the discretized Laplace equation, can be solved by iterative numerical techniques, but repeated operations are required for convergence [25]. The FPGA can implement the dedicated computational units to perform iterative techniques and can parallelize the computational units to improve throughput. Given the limited hardware resources of the chip, the reset of the issues such as solving the thermal problems and tuning physical characteristics of tissues are sequentially processed on the CPU.

4) Tuning Physical Characteristics of Tissues: For numerically solving the bio-heat equation, the electrical and thermal parameters such as electrical conductivity (σ), thermal conductivity (k), tissue density (ρ), and heat capacity (C) have been found in the literature. However, these parameters can be slightly varied depending on tissue conditions such as capillary recruitment and vasodilation or vasoconstriction [8]. To minimize the errors induced by the tissue properties, in the thermal field, we defined new parameter (q_e) regarding the error (e_{heat}) between the measure electrode temperature and the numerically calculated temperature. Therefore, q_e should ideally be 0. We bound the parameter between 0 and $q_{\max}$

$$q_e^{f+1} = q_e^f + \left(e_{\text{heat}} \times \alpha_q\right), \quad 0 < q_e < q_{\max}. \tag{7}$$

The new parameter is coupled with the bio-heat equation similar to the cooling effect term

$$Q_e^f = q_e^f \times \left(T_{r,z}^f - 310\right) \tag{8}$$

$$T_{r,z}^{f+1} = T_{r,z}^{f+1} - Q_e^f. \tag{9}$$

In addition, we modified the electrical conductivity with a tuning constant (α_c) (see Fig. 3)

$$\begin{cases} \sigma_e^{f+1} = \sigma_e^f + \alpha_c, & q_e < 0 \\ \sigma_e^{f+1} = \sigma_e^f - \alpha_c, & q_{\max} < q_e. \end{cases} \tag{10}$$

The constants α_q, $q_{\max}$, and α_c were determined in the phantom study of LRDN (see Section IV-B).

5) Approximating Thermal Lesion: The thermal lesion was approximated using cumulative equivalent minutes at 43 °C, called CEM_{43}, which normalizes various thermal histories, for example, heat temperature and duration, by applying the following formula:

$$\text{CEM}_{43} = \sum_{t=o}^{t=\text{final}} R^{(43-T)} \Delta t, \quad R = \begin{cases} 0.25, & T < 43\ ^\circ\text{C} \\ 0.5, & T \geq 43\ ^\circ\text{C} \end{cases} \tag{11}$$

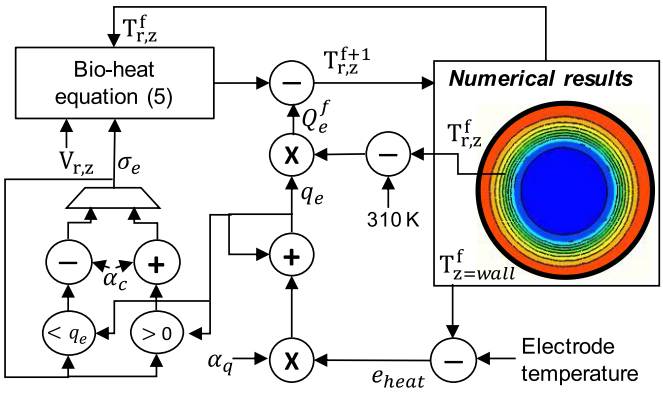

Fig. 3. Flowchart of the tuning process.

where T represents the temperature of tissue, t is the time, and R is a constant to compensate for a 1 °C rise. The threshold for deactivating various tissues, which is the thermal lesion, can be expressed using the CEM_{43}. For example, the damage threshold for an artery and nerves is a CEM_{43} of 150 min [26] and 80 min [27], respectively. Therefore, because the damage threshold on LRDN follows one on the artery (150 min) [18], the thermal duration of LRDN during surgery can be determined by considering subsurface heat, tissue types, and CEM_{43} thermal doses on each tissue.

III. Modularized RF Electrosurgical System

The proposed electrosurgical system 1) delivers RF energy to the electrodes for inducing heat in target tissues adjacent to the electrode; 2) numerically approximates the thermal lesion during treatment; and 3) displays the numerical results. To satisfy these three requirements, we proposed a modularized electrosurgical system using a hybrid solution of a CPU-FPGA on one chip and RF components. In the development of medical devices, the used components should be certified as medical devices and the equipment should pass several tests, such as dielectric withstand test and isolation test based on IEC 60601-2. Therefore, the proposed system consists of off-the-shelf components used in conventional medical devices such as medical MRI or ultrasound.

A. RF Electrosurgical System Setup

Fig. 4 shows the proposed RF electrosurgical system setup including an RF surgical instrument and a monitor. To conduct RFA, the electrosurgical system generates a 500 kHz RF signal using an RF ADC (AD9248, Analog Devices) and amplifies the signal through an RF amplifier (LZY-22+, Mini-circuits). The transmitted and reflected RF power is measured using a bidirectional coupler (ZABDC50-150HP+, Mini-circuits) and an RF DAC (AD9767, Analog Devices) which has two input ports. The temperature on an electrode is also monitored by an ADC (AD595, Analog Devices) which measures the low voltage of thermocouples. Using the transmitted and reflected power, we can derive the load impedance and the voltage on the RF electrode, which act as boundary conditions for the numerical simulation analysis. A hybrid CPU-FPGA

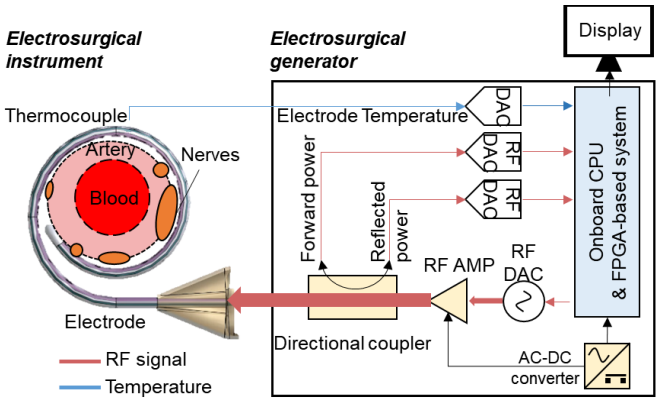

Fig. 4. Schematic representation of the electrosurgical system applicable online numerical simulation.

chip controls the system and numerically calculates the heat distribution inside an artery. All results including the heat distribution, transmitted power, and operating duration are displayed on a monitor. We used a board (DE1-SoC, Intel) comprising a monolithic integrated circuit (Cyclone V) that combines a hard processor system (HPS) and FPGA. The HPS comprises an ARM Cortex A9 dual-core processor as a CPU, on-chip memories (DDR3), and diverse peripheral devices.

B. FPGA-Based Accelerator to Solve the Laplace Equation

The electrical–thermal governing equation consists of the Laplace equation and heat equation. At each time step, numerical analysis of the Laplace equation requires thousands of iterations, whereas the heat equation only requires one computation. The iterative techniques are significantly effective when FPGA that can implement parallel processing element (PE) is used. Therefore, we solve the Laplace equation using FPGA to reduce the computing time and the heat equation on CPU.

In this computing system, we employed a 27-bit floating-point format by modifying the IEEE Standard 754. The 27-bit format consisted of a single bit sign, 8-bit exponent, and 18-bit fraction. The multiplication or addition of 18-bit fraction utilizes one DSP unit of the target FPGA (Cyclone V). In addition, because this is equivalent to a floating number in C programming by adding five zeros to the fraction of the least significant bit, FPGA can communicate with the CPU without any additional hardware design. We designed the add operation of the 27-bit format as a combinational circuit and the multiple operation as a two-stage sequential circuit.

Equation (4) was reshaped to optimize the 27-bit floating operation and to be processed by the pipelining technique

$$V_{r,z} = \frac{C_1}{r} \times \left(V_{r+1,z} - V_{r-1,z}\right) + C_2 \times \left(V_{r+1,z} + V_{r-1,z}\right) + C_3 \times \left(V_{r,z+1} + V_{r,z-1}\right) \tag{12}$$

where $C_1 = \Delta r^2 \Delta z^2 / 4\Delta r(\Delta r^2 + \Delta z^2)$, $C_2 = \Delta r^2 \Delta z^2 / 2\Delta r^2(\Delta r^2 + \Delta z^2)$, and $C_3 = \Delta r^2 \Delta z^2 / 2\Delta z^2(\Delta r^2 + \Delta z^2)$. Consequently, we designed a five-stage pipeline computing unit to solve the Laplace equation (see Fig. 5).

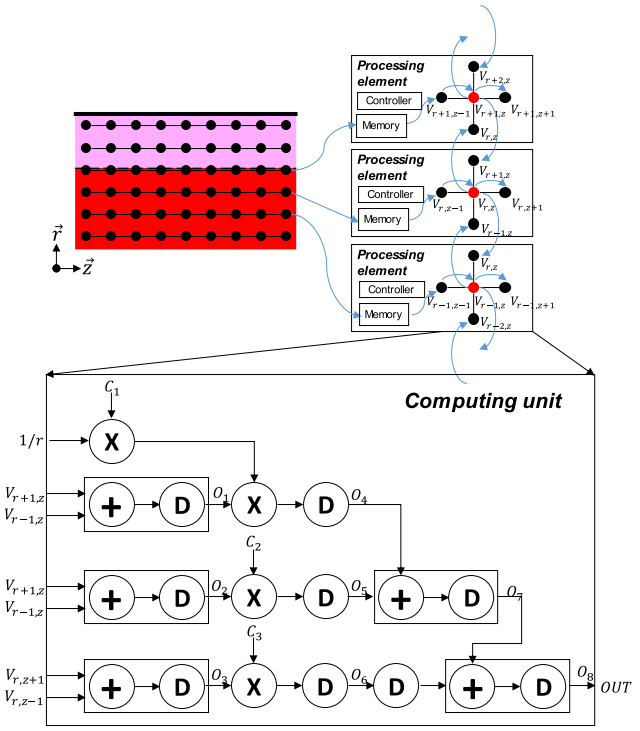

Fig. 5. Computing unit and dataflow of the parallel processing algorithm.

We generated 11 PEs in FPGA that iteratively processes a line of grids along the Z-axis (110 grids) in the 2-D computational domain.

C. Heterogeneous System on a Hybrid CPU-FPGA Chip

The hardware modules on FPGA were subdivided into five modules implemented by Verilog, and one module designed using a schematic method with Intel IPs. The programed modules of Verilog included an ADC/DAC controller, a peak-to-peak voltage calculator, an accelerator for FDTD, temperature monitoring, and a feedback controller. In addition, the modules using Intel IPs support the RF electrosurgical system to display the computing results on a monitor. Fig. 6 shows the overall implementation of the FPGA part.

The ADC/DAC controller module coordinates the operation of the RF signal generation and the measurement of the electrode voltage. It sends out control signals to the RF ADC and DAC IC through GPIOs of the DE1-SoC board. In the domain of the 50-MHz clock which generates a 500 kHz sinusoidal signal, the module sends one command signal to the DAC repeatedly 100 times per clock. The command signal is 14-bit data pre-stored in ROM and controls the amplitude of the DAC output. Meanwhile, this module receives 14-bit data from RF ADC at the 65 MHz clock. The ADC data are transmitted to the on-chip RAM in the peak-to-peak voltage calculator module. The on-chip RAM has two ports: s1 and s2. The s1 port is connected to the ADC/DAC controller module at the 65 MHz clock, and the s2 port is connected to the AXI-bus master of the CPU at the 50 MHz clock. Starting from 100 μs after generating the 500-kHz sinusoidal signal at the DAC, the RAM in the domain of the 65 MHz clock

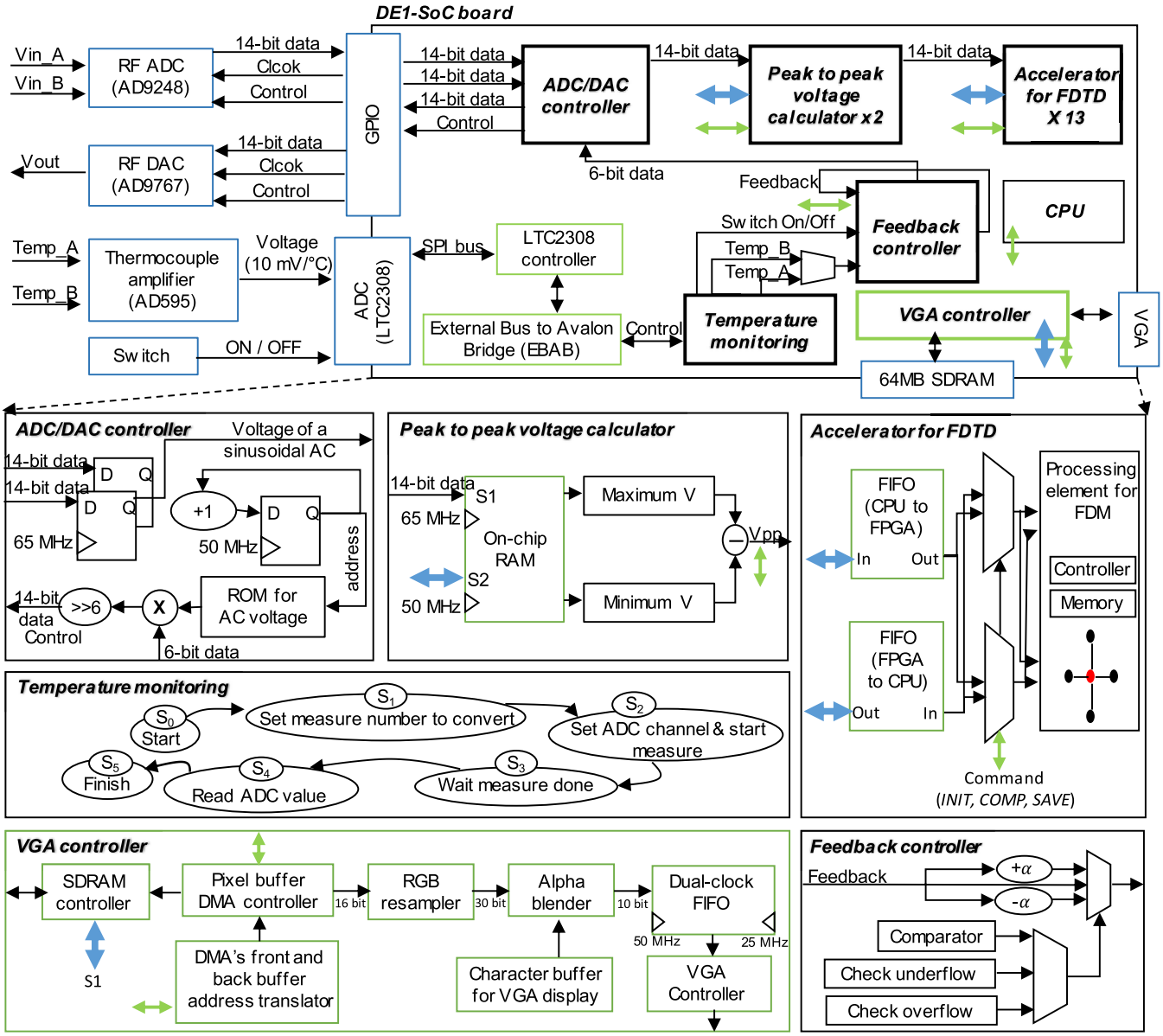

Fig. 6. Configuration of the hybrid CPU-FPGA chip. Black box is a textual programed module using Verilog, green box is a module supported by Intel, and blue box is an integrated circuit. Blue arrow is an AXI bus and green arrow is a lightweight AXI bus.

stores 128 ADC data that can store over one period of the 500 kHz signal. Therefore, the peak-to-peak voltage calculator module can find the maximum and minimum values on the received ADC data and derive the peak-to-peak voltage of the 500 kHz signal. We used two modules of the peak-to-peak voltage calculator to find the voltage of the transmitted and reflected RF energy. Finally, the peak-to-peak voltages will be used as the boundary conditions of (4) at the accelerator for the FDTD module.

The accelerator for the FDTD module, which operates at 100 MHz, embedded two first-in first-out (FIFO) buffers and a PE for FDTD. Data communication between FPGA and CPU was performed by the FIFO buffers using the AXI bus. The PE consists of a controller, an on-chip memory (M10K), and the five-stage pipelined computing unit (see Fig. 5). This module is controlled by three commands (INIT, COMP, SAVE) from CPU; INIT loads the initial voltage and boundary conditions on the on-chip memory, COMP operates the PEs, and SAVE sends out all data on the on-chip memories to the CPU.

The temperature data from AD595 can be read from the LTC2308 ADC built into the DE1-SoC board. We used an Intel IP to control the built-in ADC and connected the Avalon slave of the IP to the FPGA system with a bridge module, called the external bus to Avalon bridge (EBAB). In the FPGA system, the temperature monitoring module connects to the EBAB and can operate the LTC2303 ADC. The feedback controller module receives temperature data. This module normalizes the difference between the measured temperature and a preset target temperature to a 6-bit integer. The integer is used by

TABLE I
RESOURCE UTILIZATION OF A HYBRID CPU-FPGA CHIP

Module	ADAPTIVE LOGIC MODULE (ALM)	LUT	DSP	M10K
Accelerator for FDTD (x11)	About 2000	About 2900	4	1
Accelerator for FDTD at the boundary (x2)	About 40	About 75	0	1
Temperature monitoring	54	77	0	0
Peak to peak voltage calculator (x2)	About 117	157	0	0
ADC/DAC controller	87	119	1	0
Intel IPs	5390	9213	6	19
Total	28,283	42,924	51	41

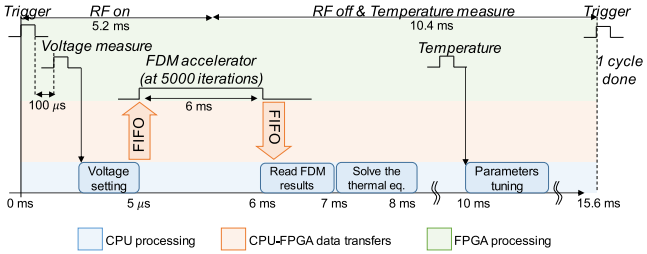

Fig. 7. Timing diagram of the hybrid CPU-FPGA chip.

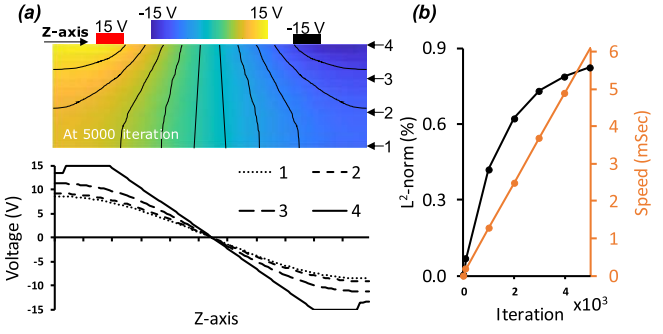

Fig. 8. (a) Calculating the Laplace equation using the FDTD accelerator after 5000 iterations. (b) L^2-norm of error and solution time at different iterations.

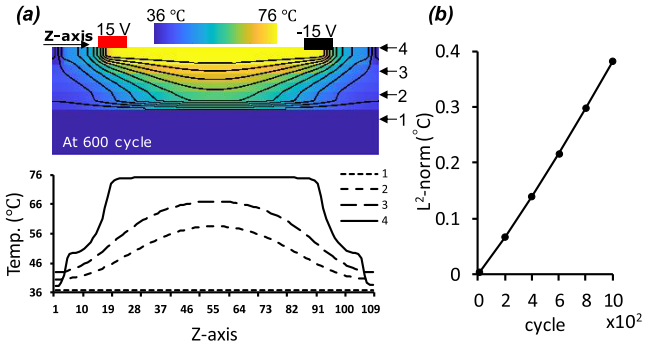

Fig. 9. (a) Calculating the bio-heat equation on the hybrid CPU-FPGA chip at 600 cycle. (b) L^2-norm of error at different cycles.

the ADC/DAC controller module to modulate the amplitude of the 500 kHz sinusoidal signal.

IV. RESULTS AND VALIDATION

A. Operation of the RF Electrosurgical System

The hybrid CPU-FPGA chip targeted the Intel Cyclone V 5CSEMA5F31C6 FPGA. This chip integrates the FPGA fabric and dual-core ARM cortex-A9 (CPU) on a single die. Table I shows the hardware resource utilization of each module on the chip. The 13 accelerators for FDTD modules solve the Laplace equation over a 2 (r-axis) $\times$ 3.85 (z-axis) mm^2 computational domain. Two module-processing grids at a radial distance of 0 (first) and 2 (last) are configured with fewer hardware resources than those used for other modules because the boundaries of the computational domain do not require a PE.

The controller of the overall system is implemented in CPU using the C application (see Fig. 7). The first step is to send a trigger signal from the CPU to the FPGA. The signal controls the ADC/DAC controller module to generate a 500 kHz RF signal and measures the voltage on the RF electrode. When the voltage measurement is complete, FPGA sends a signal to the CPU. Then, the CPU initiates the electrical boundary conditions using the measured voltage by transmitting the INIT command to the accelerator for the FDTD module and starts to calculate (4) using the FDTD accelerator by transmitting the COMP command. After the trigger signal is generated, ~7 ms are required for the accelerator to complete the operation and the CPU to receive the result. In the next step, the CPU computes (5) using the FDTD accelerator results at a time interval (Δt) of 5.2 ms (RF ON) and 0 V at a time interval of 10.4 ms (RF OFF and temperature measurement). Finally, the bio-heat equation can be solved within 10 ms after the trigger start. Before the next trigger signal starts, the CPU compares the computational result against the measured temperature and adjusts the physical characteristics of tissues to minimize the error. The time interval between two triggers is 15.6 ms, which is one cycle.

We evaluated the computing performance of the bio-heat equation by setting the electrical boundary condition as 15 V (Figs. 8 and 9). The bio-heat equation and boundary conditions were also implemented in MATLAB using an Intel Core i7-6700. The FDTD accelerator numerically solved the Laplace equation by repeating the calculation 5000 times [see Fig. 8(a)]. At 5000 iterations, the L^2-norm of the error between the FDTD accelerator (27-bit floating point) and MATLAB (64-bit floating point) numerical solution was ~0.05 V (0.82%). In addition, it takes about 6 ms when operating the accelerator at 100 MHz clock [see Fig. 8(b)] that is 2000 times that required by MATLAB (12.8 s). After solving the Laplace equation, the hybrid CPU-FPGA chip calculates the remaining thermal problems in the CPU. When computing is repeated up to 1000 cycles (15.6 s), the L^2-norm of the error between the results of the chip and results of MATLAB becomes ~0.4 °C (0.11%) [see Fig. 9(b)].

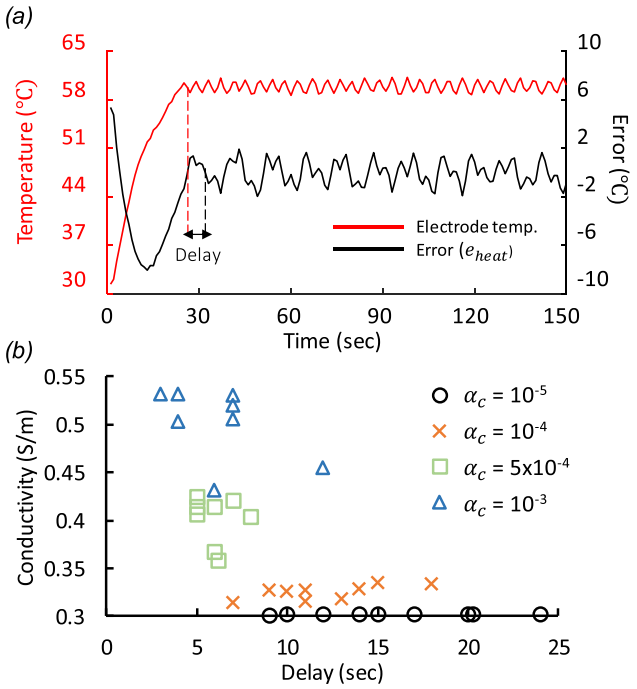

Fig. 10. (a) Profile of electrode temperature and error (e_{heat}). (b) Modified electrical conductivity on various tuning constants (α_c).

B. Phantom Experiment

We tested the RF electrosurgical system on a phantom gel fabricated by mixing 200 mL of water with 10 g of gelling agent (No. 436364, Sigma-Aldrich) and 3.3 g of sodium chloride (No. S7653, Sigma-Aldrich). The electrical conductivity could be controlled by the amount of sodium chloride, but the mass density and thermal properties were the same as those of water [18], [28]. Therefore, this phantom gel had an electrical conductivity of 0.33 S/m (at room temperature, 25 °C), which is similar to that of the human artery. The electrical conductivity is a temperature-dependent value which can be assumed to increase by 2% for a 1 °C rise [8]. In the phantom experiment, the simulation model is considered as a macro-fragment of a gel.

The experiment started at 30 °C, and the temperature of the electrode was raised to 60 °C [see Fig. 10(a)]. The maximum used to maintain the laparoscopic electrode at a constant ablation temperature during the renal denervation is 60°C [19]. The maximum has been determined empirically from our previous in-silico studies and *in vivo* studies using pigs [7], [29]. We evaluated the relationship between the actual electrode temperature and the numerical result by changing the constants of α_q, $q_{\max}$, and α_c. When α_q was 0.00001 and $q_{\max}$ was 0.05, the modified conductivity was converged. The constant α_c affected the magnitude of the conductivity [see Fig. 10(b)]. We finally determined α_c as 0.001 because the modified electrical conductivity should be 0.51 S/m at 60 °C. This shows that the conductivity modified in real-time based on temperature rise during RFA further reduces the error due to changes in tissue properties.

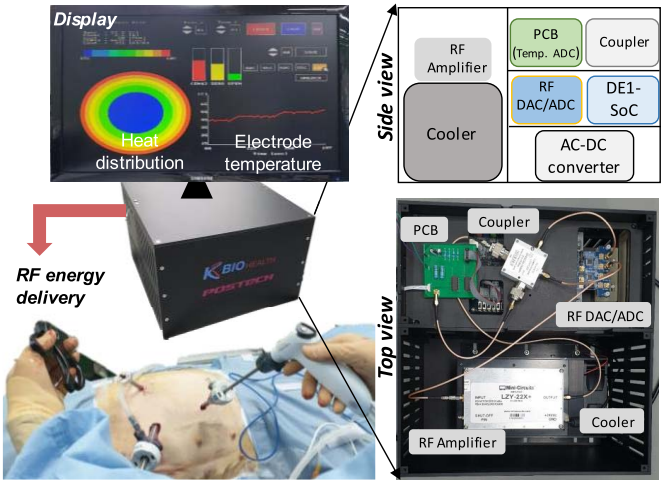

Fig. 11. Box containing the hybrid chip and RF components.

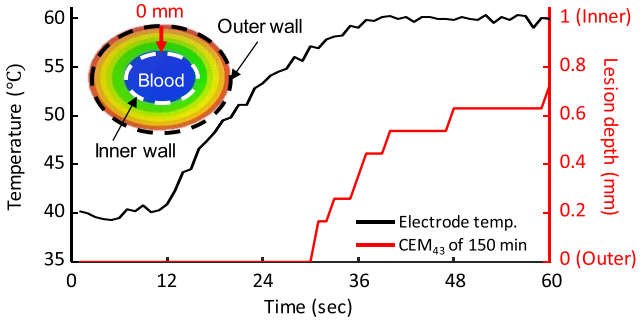

Fig. 12. Real-time thermal lesion approximation.

C. RFA on an Animal Study Using a Pig

We integrated the hybrid CPU-FPGA chip and RF components in a box (see Fig. 11). A laparoscopic electrosurgical instrument for LRDN and a monitor were connected to the box. The electrode of the laparoscopic instrument consisted of a Nitinol substrate and a flexible printed circuit board, which was proved to be safe from the previous survival animal study using pigs [7]. The feasibility of the system was demonstrated through an animal study using a swine model that mimics the human anatomy and physiology the best. We performed LRDN with this system on two main renal arteries of a pig (Movie 1). The animal experiment involved an open surgery and was approved by the Institutional Animal Care and Use Committee in the Osong Medical Innovation Foundation (KBIO-IACUC-2021-221). For the animal study, the system could keep the electrode temperature at a preset value (black line in Fig. 12). Concurrently, it approximated the thermal lesion by calculating the bio-heat equation (red line in Fig. 12). We defined the thermal lesion as the CEM$_{43}$ of 150 min, which is the damage threshold of an artery. All results were displayed on a monitor in real-time. Details of the system operation are explained in Movie 2.

V. Conclusion

We developed a novel RF electrosurgical instrument with a hybrid CPU-FPGA chip that numerically computed the bio-heat equation by solving electrical problems in FPGA and thermal problems in CPU. The instrument conducted online numerical simulation during RFA treatment following five steps: 1) simplification of the simulation model; 2) determination of the boundary conditions; 3) task allocation to computational resources; 4) online tuning of physical characteristics of tissues; and 5) approximating the thermal lesion. In addition, the system modularly implemented the functions of RF control and electrode voltage and temperature measurement using RF components. The system could anticipate a thermal lesion in 15.6 ms within a time step of real-time simulation while performing RFA treatment. Such a framework can be used in various RFA treatments for online simulation of thermal lesions. Furthermore, the hybrid chip can be applied to conventional RF equipment as long as a few boundary conditions are met, such as electrode temperature or voltage. The modularly designed system using off-the-shelf chips and RF components is highly scalable for real-world applications. In addition, each module in the system is compatible with other imaging devices and existing electrosurgical systems, making it more useful as a mix-and-match system.

The current study mainly focused on implementing a system with online computation capability to numerically simulate LRDN with a simplified main renal artery model in real-time. However, it should be noted that further development of artery models considering more realistic conditions such as the bulked blood flow and the occluded artery is required before translating the system into clinical setting. In addition, future work will include system characterization with the developed system to evaluate the accuracy of the depth and size of the lesion produced by the thermal effect of RF. Characterizing the system accuracy on those biological parameters such as lesion depth and size require a large survival animal study since it takes weeks for target tissues to recover from acute thermal shock and stabilize. We also plan to perform various case studies, such as RFA treatment in the brain, tumor, or spine.

References

[1] N. N. Massarweh, N. Cosgriff, and D. P. Slakey, "Electrosurgery: History, principles, and current and future uses," *J. Amer. College Surgeons*, vol. 202, no. 3, pp. 520–530, Mar. 2006.

[2] B. J. Wood *et al.*, "Technologies for guidance of radiofrequency ablation in the multimodality interventional suite of the future," *J. Vascular Interventional Radiol.*, vol. 18, no. 1, pp. 9–24, Jan. 2007.

[3] B. S. Peters, P. R. Armijo, C. Krause, S. A. Choudhury, and D. Oleynikov, "Review of emerging surgical robotic technology," *Surgical Endoscopy*, vol. 32, no. 4, pp. 1636–1655, Apr. 2018.

[4] A. Franzini *et al.*, "Ablative brain surgery: An overview," *Int. J. Hyperthermia*, vol. 36, no. 2, pp. 64–80, Oct. 2019.

[5] S. Mulier *et al.*, "Complications of radiofrequency coagulation of liver tumours," *Brit. J. Surg.*, vol. 89, no. 10, pp. 1206–1222, Nov. 2002.

[6] D. E. Dupuy, R. Hong, B. Oliver, and S. N. Goldberg, "Radiofrequency ablation of spinal tumors: Temperature distribution in the spinal canal," *Amer. J. Roentgenol.*, vol. 175, no. 5, pp. 1263–1266, Nov. 2000.

[7] J. Baik *et al.*, "Laparoscopic ablation system for complete circumferential renal sympathetic denervation," *IEEE Trans. Biomed. Eng.*, vol. 68, no. 11, pp. 3217–3227, Nov. 2021.

[8] E. J. Berjano, "Theoretical modeling for radiofrequency ablation: State-of-the-art and challenges for the future," *Biomed. Eng. OnLine*, vol. 5, no. 1, pp. 1–17, Dec. 2006.

[9] E. Ye *et al.*, "Design and simulation of novel laparoscopic renal denervation system: A feasibility study," *Int. J. Hyperthermia*, vol. 35, no. 1, pp. 9–18, Dec. 2018.

[10] A. R. Tzafriri *et al.*, "Arterial microanatomy determines the success of energy-based renal denervation in controlling hypertension," *Sci. Transl. Med.*, vol. 7, no. 285, p. 285, Apr. 2015.

[11] E. Besler, Y. C. Wang, and A. V. Sahakian, "Real-time radiofrequency ablation lesion depth estimation using multi-frequency impedance with a deep neural network and tree-based ensembles," *IEEE Trans. Biomed. Eng.*, vol. 67, no. 7, pp. 1890–1899, Jul. 2020.

[12] K. Barbé, C. Ford, K. Bonn, and J. Gilbert, "Toward a tissue model for bipolar electrosurgery: Block-oriented model structure analysis," *IEEE Trans. Instrum. Meas.*, vol. 66, no. 3, pp. 460–469, Mar. 2017.

[13] C. Knopf, J. Himmel, S. Klockner, K. Thelen, and O. Kanoun, "3-D potential distribution measurement in electrosurgery by a flexible multielectrode system," *IEEE Trans. Instrum. Meas.*, vol. 63, no. 10, pp. 2447–2453, Oct. 2014.

[14] N. R. Tavana and V. Dinavahi, "A general framework for FPGA-based real-time emulation of electrical machines for HIL applications," *IEEE Trans. Ind. Electron.*, vol. 62, no. 4, pp. 2041–2053, Apr. 2015.

[15] H. Radner, J. Stange, L. Büttner, and J. Czarske, "Field-programmable system-on-chip-based control system for real-time distortion correction in optical imaging," *IEEE Trans. Ind. Electron.*, vol. 68, no. 4, pp. 3370–3379, Mar. 2020.

[16] T. Liang and V. Dinavahi, "Real-time system-on-chip emulation of electrothermal models for power electronic devices via Hammerstein configuration," *IEEE J. Emerg. Sel. Topics Power Electron.*, vol. 6, no. 1, pp. 203–218, Mar. 2018.

[17] H. H. Pennes, "Analysis of tissue and arterial blood temperatures in the resting human forearm," *J. Appl. Physiol.*, vol. 1, no. 2, pp. 93–122, Jul. 1948.

[18] J. Baik *et al.*, "Laparoscopic renal denervation system for treating resistant hypertension: Overcoming limitations of catheter-based approaches," *IEEE Trans. Biomed. Eng.*, vol. 67, no. 12, pp. 3425–3437, Dec. 2020.

[19] J. Baik, S. Seo, S. Lee, S. Yang, and S.-M. Park, "Circular radiofrequency electrode with MEMS temperature sensors for laparoscopic renal sympathetic denervation," *IEEE Trans. Biomed. Eng.*, vol. 69, no. 1, pp. 256–264, Jan. 2022.

[20] D. L. Thomas, M. F. Lythgoe, G. S. Pell, F. Calamante, and R. J. Ordidge, "The measurement of diffusion and perfusion in biological systems using magnetic resonance imaging," *Phys. Med. Biol.*, vol. 45, no. 8, pp. R97–R138, Aug. 2000.

[21] S. Engdahl, *Solving the Bioheat Equation for Transcutaneous Recharging of a Medical Device Using Electric Fields*. Springfield, OH, USA: Wittenberg Univ., 2013.

[22] A. Emery and H. Mortazavi, "A comparison of the finite difference and finite element methods for heat transfer calculations," in *Proc. NASA Conf. Comput. Aspects Heat Transf.*, 1982, pp. 51–82.

[23] H. Cao *et al.*, "Flow effect on lesion formation in RF cardiac catheter ablation," *IEEE Trans. Biomed. Eng.*, vol. 48, no. 4, pp. 425–433, Apr. 2001.

[24] F. A. Duck, *Physical Properties of Tissues: A Comprehensive Reference Book*. New York, NY, USA: Academic, 2013.

[25] P. Moin, *Fundamentals of Engineering Numerical Analysis*. Cambridge, U.K.: Cambridge Univ. Press, 2010.

[26] D. C. Gross, "Improving patient safety by quantifying vascular tissue damage from radio frequency induced heating of implanted medical devices during magnetic resonance imaging," Ph.D. dissertation, Dept. Biomed. Eng., Ohio State Univ., Columbus, OH, USA, 2016.

[27] M. W. Dewhirst, B. L. Viglianti, M. Lora-Michiels, M. Hanson, and P. J. Hoopes, "Basic principles of thermal dosimetry and thermal thresholds for tissue damage from hyperthermia," *Int. J. Hyperthermia*, vol. 19, no. 3, pp. 267–294, Jan. 2003.

[28] S. M. Park *et al.*, "Gelled versus nongelled phantom material for measurement of MRI-induced temperature increases with bioimplants," *IEEE Trans. Magn.*, vol. 39, no. 5, pp. 3367–3371, Oct. 2003.

[29] J. Baik *et al.*, "Laparoscopic renal denervation system for treating resistant hypertension: Overcoming limitations of catheter-based approaches," *IEEE Trans. Biomed. Eng.*, vol. 67, no. 12, pp. 3425–3437, Dec. 2020.

Jinhwan Baik received the B.S. degree in electronic engineering from Soongsil University, Seoul, South Korea, in 2017. He is currently pursuing the Ph.D. degree with the Department of Convergence IT Engineering, Pohang University of Science and Technology (POSTECH), Pohang, South Korea.

His research interests include numerical analysis and CPU-FPGA heterogeneous platform for real-time applications.

Sangyong Lee received the Ph.D. degree from Chungnam National University, Daejeon, Republic of Korea, in 2014.

He is currently a Researcher at the OSONG Medical Innovation Foundation, Cheongju-si, Chungbuk, Republic of Korea. His research interests are the development and application of surgical and optical medical devices.

Sunchoel Yang received the Ph.D. degree majoring in mechanical engineering from Chungnam National University, Daejeon, Republic of Korea, in 2011.

He is currently working at the Medical Device Development Center, Osong Medical Innovation Foundation, as a Principal Researcher. His research interest is in the area of medical device manufacturing.

Sung-Min Park (Senior Member, IEEE) received the B.S. and Ph.D. degrees in electrical and computer engineering from Purdue University, West Lafayette, IN, USA, in 2001 and 2006, respectively.

From 2006 to 2014, he was with Medtronic, Minneapolis, MN, USA, as the Research and Development Manager, leading the award-wining effort in developing the world's first MRI conditional pacemaker. From 2014 to 2016, he was with Samsung, Suwon, South Korea, as the Director of spearheading healthcare centric mobile device and mobile health service platform development projects. He is currently a Professor with the Department of Convergence IT Engineering, Department of Electrical Engineering, and Department of Mechanical Engineering, Pohang University of Science and Technology (POSTECH), Pohang, South Korea, where he has been working since 2016.